Cooperation of Many-Body Physics and Defect Chemistry in Transition-Metal Oxides

F. Lechermann

published in

NIC Symposium 2020
M. Müller, K. Binder, A. Trautmann (Editors)

Forschungszentrum Jülich GmbH,
John von Neumann Institute for Computing (NIC),
Schriften des Forschungszentrums Jülich, NIC Series, Vol. 50,
ISBN 978-3-95806-443-0, pp. 93.
http://hdl.handle.net/2128/24435

Cooperation of Many-Body Physics and Defect Chemistry in Transition-Metal Oxides

Frank Lechermann

I. Institut für Theoretische Physik, Universität Hamburg,
20355 Hamburg, Germany
E-mail: Frank.Lechermann@physnet.uni-hamburg.de

The problem of defects in correlated materials is at the heart of the fascinating phenomenology of many of these compounds. A vast number of prominent features of strongly correlated systems, such as *e. g.* high-temperature superconductivity in cuprates and iron pnictides, or heavy-fermion physics in Ce-based compounds is often directly associated with a defect-crystal state. Already the very concept of a doped Mott-insulator builds up on the understanding of impurities implanted in an otherwise perfect crystal lattice. However, a deeper understanding of the realistic physics is then connected to a faithful description of the defect chemistry underlying the material under consideration. We here show that the combination of density functional theory (DFT) with dynamical mean-field theory (DMFT) provides a proper tool to elucidate this realistic interplay between many-body physics and defect chemistry. Focus is on transition-metal oxides which are well known to harbour diverse manifestations of electronic correlations. Two prominent concrete examples, the paramagnetic metal-to-insulator transition in V_2O_3 driven by chromium doping, and the long-standing issue of lithium-doped NiO will be addressed in some detail.

1 Introduction

Defects in crystal lattices drive very important phenomenology in condensed matter physics. Prominent examples are for instance the impurity doping of semiconductors such as silicon to facilitate conductivity or the movement of dislocations in metals as the origin for plasticity. Traditionally, one characterises such defects by their dimensionality: zero-dimensional point defects (*e. g.* vacancies or antisite atoms), one-dimensional line defects (*e. g.* dislocations) and two-dimensional planar defects (*e. g.* grain boundaries). In this brief overview, we will focus on the aspect of point defects in prominent correlated transition-metal oxides.

The effect of realistic point defects are believed to be at the root of many challenging correlation phenomena. For instance, the high-temperature superconductivity of cuprates[1] such as La_2CuO_4 or $YBa_2Cu_3O_7$ originates from hole doping the CuO_2 layers in these systems. This is realised either by directly achieving oxygen deficiency in those layers, or by introducing different-valence elements in the region in between, *e. g.* partially replacing La^{3+} by Sr^{2+} in the case of La_2CuO_4. As another example, the Ce defect compound $CeCu_{6-x}Au_x$ is a paramount case of a heavy-fermion system, possibly harbouring a quantum-critical point. Thereby, the concentration balance x between Cu and Au is a key control parameter. Furthermore, the introduction of point defects is a proper and versatile tool to modify, tune and engineer correlated materials properties in view of possible technological applications. For instance, in the areas of photovoltaic materials and battery materials, defect engineering of charge-gap sizes or redox potentials is an important optimisation procedure. Thus, a deeper realistic understanding of the interplay of electronic

correlations and defect properties is relevant from both perspectives, basic research as well as technological applications.

Of course, the theoretical modelling of point defects in materials has a long history. Yet especially for correlated materials, the tools for an investigation on a realistic level have been limited until recently. There are several limiting perspectives that are often utilised to account for the impact of defects in quantum materials. These include *e. g.* volume or lattice-parameter modifications, shifting of the chemical potential, effective-medium or virtual-crystal considerations, or the sole formation of impurity bands. While those approaches to realistic doping may provide reasonable results in certain cases, they are surely restricted, miss relevant aspects and even can be misleading. It is however also noteworthy to state that a perfectly satisfying approach does yet not exit. Randomly-distributed point defects break the translational invariance of the crystal lattice, which render usual $\mathbf{k}$-space approaches only approximate. Still, a sound first-principles modelling should be able to tackle both, local as well as long-ranged effects of the defect introduction to the lattice. Therefore, supercell approaches are generally believed to mark the best-tailored approximations to the problem. Though they necessarily introduce a periodical reproduction and hence an artificial ordering pattern of defects, this failure can in principle be converged to negligible contribution by further and further enlargement of the supercell. In practise, since a quantum-physical relevant defect impact usually arise only for concentrations $> 1\%$, supercell sizes of up to 100-200 atomic sites turn out sufficient for most materials under consideration to obtain reasonable results. Note that we here do not aim at *e. g.* metallurgical problems such a dislocation dynamics or crack propagation on an atomistic level, which often ask for more than 10^6 atoms in a (semi)classical molecular-dynamics simulation. First-principles supercell approaches enable the description of local effects, such as *e. g.* local distortions or local symmetry breakings, and global effects, such as *e. g.* lattice-parameter changes or modifications of the lattice electronic structure.

2 Theoretical approach: multi-site DFT+DMFT

The proper first principles approach for defects in correlated materials asks for the following ingredients. A faithful description of the chemical bonding and lattice effects, a general and accurate account of many-body physics, both with reasonable numerical performance in a supercell architecture. The charge self-consistent combination of density functional theory (DFT) with dynamical mean-field theory (DMFT) in a multi-site or so-called "real-space" setting fits to these demands. We here provide only a brief review of the DFT+DMFT framework, more detailed descriptions can be found elsewhere (*e. g.* Ref. 2).

Key to DFT+DMFT is the interfacing of both methods, usually realised by subsequent down- and upfolding between a general Bloch space and a chosen correlated subspace $\mathcal{C}$. The Kohn-Sham DFT treatment of the problem covers the whole Bloch space, while DMFT is explicitly active only in $\mathcal{C}$. Charge self-consistency via an update of the Kohn-Sham potential by including DMFT self-energy effects for the charge density, ensures a thorough coupling within this hybrid scheme. The correlated subspace is obtained from a Wannier(-like) construction for the correlation-relevant quantum space. The d shell of transition metals or the f shell of rare-earth atoms usually form the latter, if they actively take part in the charge fluctuations within the system. Locally, a multi-orbital Hubbard Hamiltonian is applied $\mathcal{C}$, usually parametrised in a spherical form by a Hubbard interaction

U and a Hund's exchange J_{H}.

In the supercell approach, the correlated subspace spans over all correlated sites, whereby each of these sites defines an impurity problem in the DMFT sense.[3] The coupling is realised via the DFT+DMFT self-consistency condition invoking the computation of the complete lattice Green's function. This multi-site or real-space framework generalises DMFT to the problem of various coupled single-site impurity problems on a given lattice. Note that it is only necessary to explicitly compute the impurity self-energy on symmetry-inequivalent sites and then translate the self-energy to the equivalent sites.

The results discussed here were obtained with a mixed-basis pseudopotential code[4] for the DFT part and by hybridisation-expansion continous-time quantum Monte Carlo (CT-QMC)[5] as implemented in the TRIQS package[6] for the DMFT impurity solution. For more technical details on the DFT+DMFT implementation the reader is referred to Ref. 2. The computational effort scales with the number of inequivalent sites to be treated in DMFT, the CT-QMC part marking the main bottleneck of the calculation. However, the DFT part of the problem may also become demanding in the supercell approach. Note that computationally, the calculations are challenging from both aspects, numerical performance as well as memory issues.

3 Cr and Ti doping of V_2O_3

The phase diagram of V_2O_3[7–9] (see Fig. 1) poses a sophisticated condensed-matter problem for about 50 years. The correlated oxide at stoichiometry is a paramagnetic metal (PM) at ambient conditions, but transforms into an antiferromagnetic insulator (AFI) well below 200 K. Application of pressure as well as doping with Ti stabilises the PM phase. Doping with Cr leads to a paramagnetic insulator (PI) at a certain concentration threshold. Measurements show that the introduction of Cr expands furthermore the lattice. Therefore, to a first approximation, doped V_2O_3 has long been thought as a realistic case of a canonical Mott system: applied pressure leads to strong hybridisation and hence stronger metallicity, while negative pressure strengthens the localisation tendencies, hence stabilises the Mott

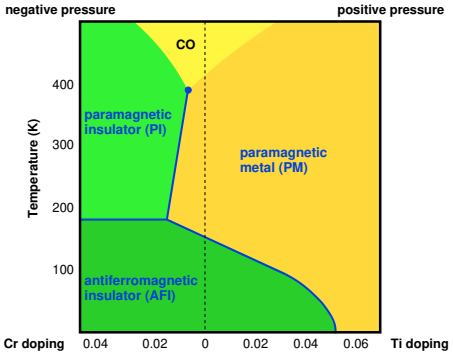

Figure 1. Experimental phase diagram of V_2O_3 as given by Refs. 7–9. Paramagnetic metal (PM) at ambient conditions and with Ti doping, paramagnetic insulator (PI) with Cr doping and at negative pressure, antiferromagnetic insulator (AFI) at low temperature.

insulator. The localised spin degree furthermore orders antiferrormagnetically at low T due to the well-known kinetic-exchange mechanism.

However based on further experimental facts[10] and recent DFT+DMFT calculations,[2, 11–14] it has become clear that this appealing simplistic picture falls too short. For instance, it has long been shown that the Ti doping also expands the lattice,[15] though not that strongly as Cr doping. This is an important lesson: though applied pressure and Ti doping have the same principal effect on the conductivity, that does not immediately mean that the physical reason behind is identical, *i. e.* that both processes contract the lattice. Furthermore, the recent DFT+DMFT[14] study revealed that for reasonable local Coulomb interactions the lattice-expansion effect in the Cr-doped case alone cannot account for the appearance of the PI phase. Thus there has to be something more to both doping scenarios, in order to explain the long-standing phase-diagram findings. We here briefly review the key content of Ref. 14, and refer to the original publication for further details.

The DFT+DMFT investigation was performed with using the V$(3d)$-t_{2g} threefold orbital sector, *i. e.* two e_g^π and one a_{1g} orbital, as the local correlated subspace. A Slater-Kanamori Hamiltonian parametrised by $U = 5\,\mathrm{eV}$ and $J_\mathrm{H} = 0.7\,\mathrm{eV}$ governs that space. The doping scenarios are realised by 80-atom supercells, where one V site is replaced by Cr or Ti, respectively (see Fig. 2a). This amounts to a defect concentration of 3.1 %, matching experimental reality. Structural relaxation of the defect cells is performed within DFT+U. Fig. 2b/c summarise the key findings of the theoretical study at $T = 194\,\mathrm{K}$. The stoichiometric reference phase is verified metallic with sizeable correlations, visible by the clear formation of lower and upper Hubbard bands in line with a renormalised quasiparticle

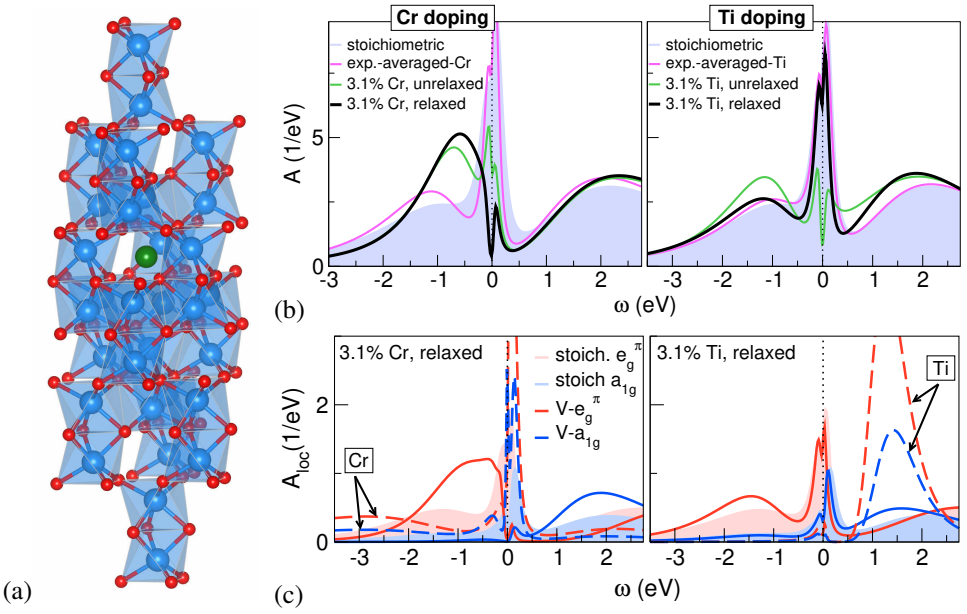

Figure 2. Theoretical modelling of 3.1 % Cr or Ti doping of V_2O_3. (a) 80-atom supercell with V (blue), O (red) and impurity (green). (b,c) DFT+DMFT result for the total (b) and local (c) spectral function for various settings at $T = 194\,\mathrm{K}$.

(QP) peak at the Fermi level. On the local level, there is polarisation towards e_g^π, slightly enhanced compared to the orbital polarisation within DFT.

Let's then focus first on the Cr doping. The simplest treatment is still performed in the original small primitive cell, but using the experimental averaged lattice data that comes with the Cr-induced expansion. Correlations are further enhanced within this picture, yet an insulating regime may not be realised. Next, a supercell calculation with still unrelaxed atomic positions already leads to a further substantial spectral-weight transfer and a weakened QP peak. Thus the sole substitution of V by non-isovalent Cr already leads to charge fluctuations/transfers and symmetry reduction in the system, and increases electronic correlations. Additional structural relaxations finally lead to the opening of charge gap of size $\sim 0.1\,\mathrm{eV}$ in good agreement with experimental results.[16, 17] The local spectral functions show finally a very strong orbital polarisation towards e_g^π, which qualitatively also matches with an experimental comparison between the stoichiometric and the Cr-doped phase.[18] The chromium site nonetheless essentially remains in the expected Cr^{3+} state, with its t_{2g} states located around $\sim -2.5\,\mathrm{eV}$. However, fluctuations with the host atoms are still very strong, as evidenced by a strong Cr resonance just above the charge gap. The key reason for the Mott-insulating instability with Cr doping are local symmetry breakings from trigonal to monoclinic that occur upon structural relaxation. Thereby, the degeneracy of both e_g^π states is lifted and the strong correlations are then very effective in driving the system towards the insulating regime.

Turning to the Ti-doped case, the physics is quite different. The introduction of Ti leads in the end to a correlated metal, in agreement with experiment. The Ti-t_{2g} states are well above the Fermi level, hence one is facing a Ti^{4+} oxidation state. In other words, the titanium impurity is in a $3d^0$ state and effectively dopes its surrounding with one additional electron. From a low-temperature perspective, this charge-doping effect of Ti renders Mott-insulating V_2O_3 eventually metallic and prohibits insulating tendencies also at higher temperatures. Note that upon structural relaxation, the local monoclinic distortions that take place for Cr doping are absent in the Ti-doped case.

This essential differences for Cr and Ti doping explain the key features of the experimental V_2O_3 phase diagram. It becomes very clear that albeit the trends with doping seem to roughly match with a simplistic lattice expansion *vs.* contraction picture, the underlying physics is much more subtle.

4 Li doping of NiO

In the second application to be discussed in this brief review we want to focus on the late transition-metal oxide NiO. Contrary to early transition-metal oxides like V_2O_3, the charge-transfer energy Δ is much smaller in late transition-metal oxides, therefore a charge gap with correlations is often set by Δ, and charge-transfer insulators instead of Mott-Hubbard insulators are realised.[19] For NiO indeed $U > \Delta$ holds, and the O$(2p)$ states reside in between the lower and upper Hubbard band of the Ni$(3d)$ states.[20] Yet Mott-Hubbard physics is still also a vital player in determining the correlated electronic structure for the insulator with a charge gap of $\sim 4\,\mathrm{eV}$. Replacing part of Ni by Li in nickel oxide has long been known to be effective in hole doping the compound.[21, 22] Recently, doped NiO gained renewed interest in view of photovoltaic applications,[23, 24] since pronounced in-gap states (IGS) appear at $\sim 1.2\,\mathrm{eV}$.[25, 26]

Here, we briefly review the recent first-principles many-body study of Li-doped NiO, for further details we refer to Ref. 27. In order to account for the stoichiometric and doped electronic spectrum of NiO with state-of-the-art DFT+DMFT, the charge-transfer tendencies have to be reasonably described. This means not only the electronic correlations emerging from Ni$(3d)$, but also from O$(2p)$ have to be described beyond DFT. Yet a full many-body account treatment of those ligand states together with the ones from the transition-metal sites proves cumbersome for various reasons. A simpler static handling of the O$(2p)$ correlations is sufficient to a good approximation. In our DFT+sicDMFT approach this is achieved by applying a self-interaction correction (SIC) to the O$(2s)$ and O$(2p)$ states on a pseudopotential level within a complete charge self-consistent DFT+DMFT scheme. This is very efficient since it does not ask for a major change of the existing self-consistency procedure, and boils down to only one additional α parameter for the SIC of O$(2p)$. The latter is chosen $\alpha = 0.8$ and should hold for a wide range of transition-metal oxides. The DMFT correlated subspace consists still of the relevant transition-metal orbital, *i. e.* here the complete Ni$(3d)$ shell, with a nominal $3d^8$ filling for present Ni^{2+}. A full Slater-Condon 5-orbital Hamiltonian for $U = 10\,\text{eV}$ and $J_\text{H} = 1.0\,\text{eV}$ acts in the correlated subspace. Since Li can be doped at rather large amounts into NiO, we choose a doping level of $x = 0.125$ for $\text{Li}_x\text{Ni}_{1-x}\text{O}$ (see Fig. 3a).

Fig. 3b shows that we indeed find the IGS essentially right at the experimentally known position of 1.2 eV. Also the further features of the stoichiometric and doped spectrums agree to a very large extent with the experimental data .[20, 25, 26] Moreover, it can be revealed that the formation of the IGS is at the expense of part of the competing correlated charge-transfer states, *i. e.* d^8 and ligand hole as well as Zhang-Rice doublet, in NiO.

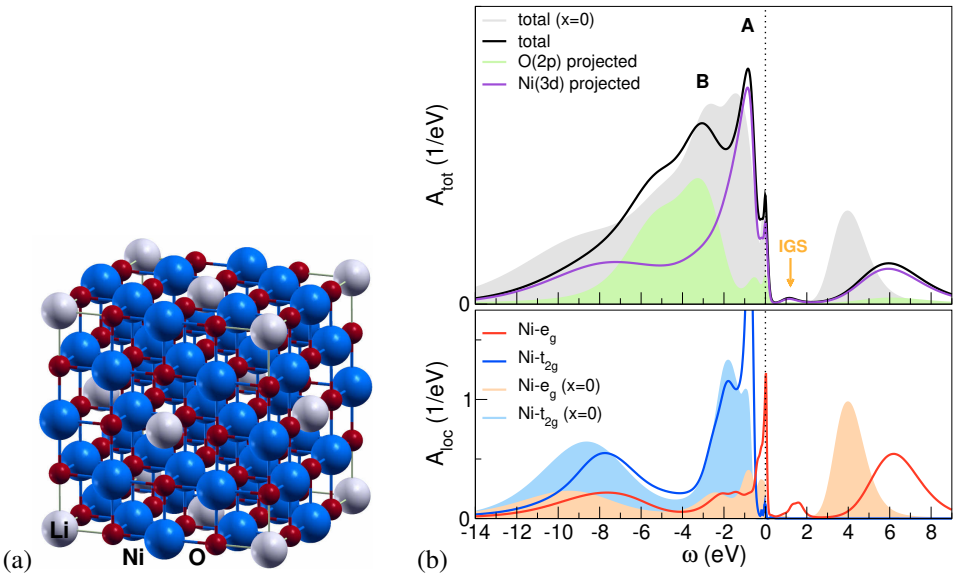

Figure 3. Theoretical modelling of 12.5 % Li doping of NiO. (a) 16-atom supercell with Ni (blue), O (red) and Li (grey). (b) DFT+sicDMFT result for the stoichiometric and doped case: total (top) and local (bottom) spectral function at $T = 582\,\text{K}$.

5 Summary

It was shown that state-of-the-art DFT+DMFT as well as its extension to DFT+sicDMFT, represent powerful tools to tackle prominent point-defect problems in correlated materials. The results underline furthermore the often underrated very important effects of dopants, sometimes referred to as "dirt". Working with this "dirt" is an indispensable way to tailor, tune and engineer correlated materials, and a deeper understanding of the associated physics inevitable for designing new states of matter in the future.

Acknowledgements

Financial support from the DFG project "Design of strongly correlated materials" LE 2446/4-1 is acknowledged. Computations were performed at the University of Hamburg and the JURECA/JUWELS Clusters of the Jülich Supercomputing Centre (JSC) under project number hhh08.

References

1. J. G. Bednorz and K. A. Müller, *Possible highTc superconductivity in the Ba-La-Cu-O system*, Z. Physik B – Condensed Matter **64**, 189, 1986.
2. D. Grieger, C. Piefke, O. E. Peil, and F. Lechermann, *Approaching finite-temperature phase diagrams of strongly correlated materials: A case study for V_2O_3*, Phys. Rev. B **86**, 155121, 2012.
3. M. Potthoff and W. Nolting, *Surface metal-insulator transition in the Hubbard model*, Phys. Rev. B **59**, 2549, 1999.
4. B. Meyer, C. Elsässer, F. Lechermann, and M. Fähnle, "Fortran 90 program for mixed-basis-pseudopotential calculations for crystals".
5. P. Werner, A. Comanac, L. de' Medici, M. Troyer, and A. J. Millis, *Continuous-time solver for quantum impurity models*, Phys. Rev. Lett. **97**, 076405, 2006.
6. P. Seth, I. Krivenko, M. Ferrero, and O. Parcollet, *TRIQS/CTHYB: A continuous-time quantum Monte Carlo hybridisation expansion solver for quantum impurity problems*, Comput. Phys. Commun. **200**, 274, 2016.
7. D. B. McWhan, T. M. Rice, and J. B. Remeika, *Mott Transition in Cr-Doped V_2O_3*, Phys. Rev. Lett. **23**, 1384, 1969.
8. D. B. McWhan, J. B. Remeika, T. M. Rice, W. F. Brinkman, J. P. Maita, and A. Menth, *Electronic Specific Heat of Metallic Ti-Doped V_2O_3*, Phys. Rev. Lett. **27**, 941, 1971.
9. D. B. McWhan, A. Menth, J. B. Remeika, T. M. Rice, and W. F. Brinkman, *Metal-Insulator Transitions in Pure and Doped V_2O_3*, Phys. Rev. B **7**, 1920, 1973.
10. I. Lo Vecchio, J. D. Denlinger, O. Krupin, B. J. Kim, P. A. Metcalf, S. Lupi, J. W. Allen, and A. Lanzara, *Fermi Surface of Metallic V_2O_3 from Angle-Resolved Photoemission: Mid-level Filling of e_g^π Bands*, Phys. Rev. Lett. **117**, 166401, 2016.
11. D. Grieger and F. Lechermann, *Effect of chromium doping on the correlated electronic structure of V_2O_3*, Phys. Rev. B **90**, 115115, 2014.
12. X. Deng, A. Sternbach, K. Haule, D. Basov, and G. Kotliar, *Shining light on transition-metal oxides: unveiling the hidden fermi liquid*, Phys. Rev. Lett. **113**, 246404, 2014.

13. I. Leonov, V. I. Anisimov, and D. Vollhardt, *Metal-insulator transition and lattice instability of paramagnetic V_2O_3*, Phys. Rev. B **91**, 195115, 2015.
14. F. Lechermann, N. Bernstein, I. I. Mazin, and R. Valentí, *Uncovering the Mechanism of the Impurity-Selective Mott Transition in Paramagnetic V_2O_3*, Phys. Rev. Lett. **121**, 106401, 2018.
15. S. Chen, J. E. Hahn, C. E. Rice, and W. R. Robinson, *The effects of titanium or chromium doping on the crystal structure of V_2O_3*, J. of Solid State Chem. **44**, 192, 1982.
16. A. S. Barker Jr. and J. P. Remeika, *Optical properties of V_2O_3 doped with chromium*, Solid State Comm. **8**, 1521, 1970.
17. S.-K. Mo, H.-D. Kim, J. D. Denlinger, J. W. Allen, J.-H. Park, A. Sekiyama, A. Yamasaki, S. Suga, Y. Saitoh, T. Muro, and P. Metcalf, *Photoemission study of $(V_{1-x}M_x)O_3$ (M=Cr, Ti)*, Phys. Rev. B **74**, 165101, 2006.
18. J.-H. Park, L. H. Tjeng, A. Tanaka, J. W. Allen, C. T. Chen, P. Metcalf, J. M. Honig, F. M. F. de Groot, and G. A. Sawatzky, *Spin and orbital occupation and phase transitions in V_2O_3*, Phys. Rev. B **61**, 11506, 2000.
19. J. Zaanen, G. A. Sawatzky, and J. W. Allen, *Band gaps and electronic structure of transition-metal compounds*, Phys. Rev. Lett. **55**, 418, 1985.
20. G. A. Sawatzky and J. W. Allen, *Magnitude and origin of the band gap in NiO*, Phys. Rev. Lett. **53**, 2339, 1984.
21. R. R. Heikes and W. D. Johnston, *Mechanism of Conduction in Li-Substituted Transition Metal Oxides*, J. Chem. Phys. **26**, 582, 1957.
22. J. B. Goodenough, D. G. Wickham, and W. J. Croft, *Some magnetic and crystallographic properties of the system $Li_x^+Ni_{1-2x}^{++}Ni_x^{+++}O$*, J. Phys. Chem. Solids **5**, 107, 1958.
23. J. Y. Jeng, K. C Chen, T. Y. Chiang, P. Y Lin, T. D Tsai, Y. C Chang, T. F Guo, P. Chen, T. C. Wen, and Y. J. Hsu, *Nickel Oxide Electrode Interlayer in $CH_3NH_3PbI_3$ Perovskite/PCBM Plana-Heterojunction Hybrid Solar Cells*, Adv. Mater. **26**, 4107, 2014.
24. W. Chen, Y. Wu, Y. Yue, J. Liu, W. Zhang, X. Yang, H. Chen, E. Bi, I. Ashraful, M. Grätzel, and L. Han, *Efficient and stable large-area perovskite solar cells with inorganic charge extraction layers*, Science **350**, 944, 2015.
25. J. van Elp, H. Eskes, P. Kuiper, and G. A. Sawatzky, *Electronic structure of Li-doped NiO*, Phys. Rev. B **45**, 1612, 1992.
26. J. Y. Zhang, W. W. Li, R. L. Z. Hoye, J. L. MacManus-Driscoll, M. Budde, O. Bierwagen, L. Wang, Y. Du, M. J. Wahila, L. F. J. Piper, T.-L. Lee, H. J. Edwards, V. R. Dhanak, and K. H. L. Zhang, *Electronic and transport properties of Li-doped NiO epitaxial thin films*, J. Mater. Chem. C **6**, 2275, 2018.
27. F. Lechermann, W. Körner, D. F. Urban, and C. Elsässer, *Interplay of charge-transfer and Mott-Hubbard physics approached by an efficient combination of self-interaction correction and dynamical mean-field theory*, Phys. Rev. B **100**, 115125, 2019.